AGU100 ADVANCING EARTH AND SPACE SCIENCE

JGR Atmospheres

RESEARCH ARTICLE
10.1029/2019JD030771

Special Section:
Bridging Weather and Climate: Subseasonal-to-Seasonal (S2S) Prediction

Evaluating the Joint Influence of the Madden-Julian Oscillation and the Stratospheric Polar Vortex on Weather Patterns in the Northern Hemisphere

Matthew R. Green[1] and **Jason C. Furtado**[1]

[1]School of Meteorology, The University of Oklahoma, Norman, OK, USA

Key Points:
- Pacific winter weather patterns are more related to the phase of the MJO than the polar vortex, and vice versa for the Atlantic/Europe
- Using both the MJO and the polar stratospheric vortex may improve subseasonal winter weather forecasts, compared to using them separately
- Depending on the phase of the MJO, its influences on tropospheric weather patterns may or may not involve a stratospheric pathway

Correspondence to:
M. R. Green and J. C. Furtado,
mrgreen@ou.edu;
jfurtado@ou.edu

Citation:
Green, M. R., & Furtado, J. C. (2019). Evaluating the joint influence of the Madden-Julian oscillation and the stratospheric polar vortex on weather patterns in the Northern hemisphere. *Journal of Geophysical Research: Atmospheres*, *124*, 11,693–11,709. https://doi.org/10.1029/2019JD030771

Received 5 APR 2019
Accepted 7 SEP 2019
Accepted article online 10 SEP 2019
Published online 17 NOV 2019

Abstract Subseasonal-to-seasonal (S2S) forecasts of Northern Hemisphere (NH) extratropical winter weather patterns continue to be a challenging venture. Past studies have considered the individual influence of two modes of climate variability—the Madden-Julian oscillation (MJO) and the state of the stratospheric polar vortex (SPV)—on the NH polar jet stream and associated weather regimes. This study takes a different approach and quantifies the joint influence of the SPV and the MJO on NH S2S winter weather patterns. Using ERA-Interim, we illustrate that variability associated with the MJO primarily influences tropospheric patterns across the North Pacific and western North America 10 to 14 days later, while SPV variability has a stronger influence on tropospheric patterns over the North Atlantic and Europe for the same lags. Over the rest of North America and into the Arctic, however, constructive and destructive interference between the MJO and the SPV teleconnections yields unique jet stream and temperature patterns that differ from the single-mode composites. As such, S2S forecasts of temperature and jet stream patterns across much of North America may improve in accuracy by considering both modes. The study also shows that MJO Phases 2 and 3 events influence the resulting tropospheric circulation via primarily a tropospheric pathway. By contrast, MJO Phases 7 and 8 events modify both the tropospheric and stratospheric circulation with potential feedbacks on the tropospheric circulation at longer lags. Hence, the study suggests another benchmark by which to test S2S dynamical prediction systems, including the importance for modeling stratosphere-troposphere coupling dynamics correctly.

1. Introduction

Winter weather patterns over the Northern Hemisphere (NH) are characterized and influenced by a number of internal modes of climate variability. On the subseasonal-to-seasonal (S2S) timescale, two particular modes of interest are the strength of the NH stratospheric polar vortex (SPV) and the Madden-Julian oscillation (MJO; e.g., L'Heureux & Higgins, 2008; Madden & Julian, 1971, 1994; Moore et al., 2010, and others). While the current state of climate science and operational S2S forecasting often consider the influences of the MJO and the SPV on the tropospheric circulation separately, using multiple modes of variability collectively has the potential to improve S2S forecast skill (e.g., Vitart et al., 2012). Thus, we must understand the dynamics behind each mode both separately and jointly.

Turning first to the stratosphere as a source of extended S2S predictability skill, several studies have focused on both the strength and position of the SPV to elucidate projected changes in the tropospheric jet stream on S2S timescales (e.g., Baldwin & Dunkerton, 2001; Scaife et al., 2014, 2016; Thompson et al., 2002). The SPV is an annular circulation that forms during the boreal cold season (e.g., October–April) at high latitudes in the NH due to strong radiational cooling. The cyclonic circulation is highly variable especially during the boreal winter (e.g., December–February; Thompson & Wallace, 2000), as the stratospheric flow is occasionally disturbed by vertically propagating Rossby waves from the troposphere (e.g., Charney & Drazin, 1961; Matsuno, 1971). Following periods of either anomalously strong or weak westerly winds in the NH polar stratosphere, same-signed anomalies descend from the extratropical stratosphere into the troposphere, changing the strength and position of the tropospheric polar jet stream (e.g., Baldwin & Dunkerton, 1999; 2001; Haynes et al., 1991; Kidston et al., 2015). The impact of these strong and weak events can last up to 60 days after they start (Baldwin & Dunkerton, 2001), yielding enhanced S2S predictability skill for NH extratropical winter weather regimes. For example, following weak vortex events, the tropospheric polar jet stream exhibits an equatorward shift in its mean position and more high-amplitude, meridional flow.

This shift subsequently changes the storm tracks across the NH and increases the chance for blocking episodes and extreme cold air outbreaks into the NH midlatitudes (e.g., Baldwin & Dunkerton, 2001; Baldwin et al., 2003; Thompson & Wallace, 2001; Waugh et al., 2017; Woollings et al., 2008).

Another internal mode of variability typically used for S2S forecasts in the NH is the MJO. The MJO is represented by areas of enhanced convection and associated strong subsidence that propagates eastward, starting in the Indian Ocean and circumnavigating the globe in the tropics over 30–90 days (Madden & Julian, 1971; Lau & Waliser, 2012; Zhang, 2005). Interaction with extratropical patterns occur as a result of Rossby wave trains generated from the anomalous convection associated with the MJO that subsequently propagate poleward (e.g., Matthews et al., 2004; Moore et al., 2010; Roundy, 2012; Seo et al., 2016; Seo & Lee, 2017). The location of the convection is characterized by phases, commonly defined by the Wheeler and Hendon Real-Time Multivariate MJO (RMM) Index (Wheeler & Hendon, 2004). For example, MJO Phases 2–3 are when tropical convection is anomalously strong in the Indian Ocean, while MJO Phases 7–8 are when convection is strong in the central tropical Pacific Ocean.

Because of its influences on extratropical tropospheric wave patterns (Moore et al., 2010), several studies have analyzed the interaction between the MJO and other NH extratropical modes of climate variability. Works by L'Heureux and Higgins (2008), Lin et al. (2009), and Jiang et al. (2017), for example, found that MJO Phases 2, 3, and 4 (7 and 8) were more frequently associated with a positive (negative) Arctic oscillation/Northern Annular Mode (NAM; Thompson & Wallace, 1998, 2000) regime. Cassou (2008) showed skillful predictions of the North Atlantic oscillation (NAO; e.g., Barnston & Livezey, 1987; Hurrell, 1996; Walker & Bliss, 1932) with lead times of almost 2 weeks when using the MJO phase and its amplitude as a predictor. The positive phase of the Pacific-North American pattern (PNA; e.g., Barnston & Livezey, 1987; Seo et al., 2016; Seo & Lee, 2017; Trenberth et al., 1998) is frequently found after MJO Phase 4 events and before MJO Phase 6 events, along with increased frequency of European blocking episodes (Frederiksen & Lin, 2013; Henderson et al., 2016).

Thus far, most of the climate and S2S forecasting literature have focused on examining the influence of the SPV and MJO on the extratropical flow pattern separately. However, in reality, these two modes (and others) work jointly to shape the NH wintertime tropospheric circulation. As such, this study seeks to understand better and diagnose the joint influence of both the MJO and the SPV on the NH extratropical patterns on subseasonal timescales. This increased understanding subsequently can be used operationally to improve predictability of temperature and precipitation regimes across North America and Europe. Our main hypothesis for this work is that considering the joint influence of the MJO and SPV on tropospheric weather patterns will produce different teleconnections compared to using either mode independently. The work is guided by three central research questions:

1. How do NH extratropical weather patterns (e.g., midtropospheric heights and surface temperature patterns) differ when considering only the MJO, only the SPV, and both?
2. How do the joint influences of the two climate modes vary regionally across the NH?
3. Do the MJO and the SPV work independently of one another to influence weather patterns, or are they acting on one another first before influencing the tropospheric weather patterns?

This manuscript is organized as follows. The data and methodology are presented in section 2. Then, in section 3, we quantify the single versus joint-event characteristic patterns of the MJO and the SPV via composites of several geophysical variables. Section 4 investigates the impact of the MJO on the stratosphere as an attempt to partially address potential MJO-SPV direct interactions. A discussion and summary of our results, including S2S forecasting implications, follow in section 5.

2. Methodology

2.1. Data

This study uses 39 years (1979–2017) of daily-mean data from the European Centre for Medium-Range Weather Forecasts Re-Analysis Interim data set (Dee et al., 2011). Atmospheric variables such as geopotential height (GPH), zonal winds (U), and surface air temperature (SAT) are analyzed, each with a horizontal resolution of 1.5° × 1.5° on a longitude/latitude grid. GPH and U exist on 23 vertical pressure levels from 1,000 to 1 hPa, with at least 10 levels in the high-latitude stratosphere, thus providing sufficient stratospheric resolution for us to conduct this study. We also calculate Eliassen-Palm (EP) fluxes (Edmon et al., 1980) to investigate wave propagation and stratosphere-troposphere coupling (section 4). Our study focuses on the months of October–March, as these are the months in which the MJO most actively impacts NH extratropical weather and is also the active season for NH stratosphere-troposphere dynamical coupling (e.g., Kidston et al., 2015; Thompson & Wallace, 2000). Anomalies are computed by subtracting the 30-year (1981–2010) daily climatology from each corresponding daily-mean value. Anomalies are then linearly detrended before computing statistics to avoid any bias from long-term trends on temporal statistics.

For this study, the MJO is defined using the Outgoing Longwave Radiation (OLR) MJO Index (OMI; Kiladis et al., 2014), available from the National Oceanic and Atmospheric Administration Earth System Research Laboratory. This index uses solely OLR, a measure of tropical convection, to quantify the MJO. This approach differs from the Wheeler and Hendon (2004) index, which uses OLR and 200- and 850-hPa winds to characterize the MJO. Because of the inclusion of wind in its calculation, the RMM method has the potential to identify MJO events from the wind pattern alone, whereas the OMI method identifies events from the MJO convection directly. As Rossby wave trains originate from tropical convection, we choose to use the OMI over the RMM index. The OMI uses a 20- to 96-day filtered OLR projection onto the daily spatial patterns of the empirical orthogonal function of the 30- to 96-day eastward filtered OLR (i.e., isolating eastward moving waves; Kiladis et al., 2014). The projection of the OLR onto the first and second leading empirical orthogonal functions provide two principal component (PC) time series, much like RMM1 and RMM2 from the Wheeler and Hendon (2004) index. For the OMI, the negative of the OMI-PC1 corresponds to RMM-PC2, and OMI-PC2 corresponds to the RMM-PC1. The phase and amplitude of the MJO are derived from the OMI in a similar manner set forth by Wheeler and Hendon (2004). However, when using the OMI to categorize the position and strength of the MJO, there are a few caveats that must be considered. For example, when projecting observations onto the OMI-PCs, other features of tropical convection might influence the index, such as other Kelvin waves (e.g., Roundy et al., 2009) and effects of the El Niño-Southern Oscillation on MJO activity (e.g., Hendon et al., 2007; Kessler, 2001; Wang et al., 2018). These caveats are understood as we analyze our results.

The NAM index is used to quantify the state of the stratospheric circulation (i.e., the SPV) and is defined as the leading PC time series of October–March GPH anomalies at each pressure level from the ERA-Interim reanalysis (Thompson & Wallace, 2000). For this study, the 100-hPa level NAM index (NAM_{100}) is used to characterize SPV events. This pressure level allows us to capture strong and weak SPV events that are most likely to propagate down into the troposphere. Conclusions of the study are robust (albeit with some different events) when using 50 hPa to define events for compositing (not shown).

2.2. Composite Analysis and Statistical Significance

For our composite analyses, we define “events” using the following criteria. First, both the NAM_{100} index and the OMI (amplitude) are standardized using the 1981–2010 base period. An MJO event is then defined when the amplitude of the OMI exceeds 1σ. For SPV events, a strong (weak) SPV is defined when $NAM_{100} \geq 1\sigma$ ($NAM_{100} \leq -1\sigma$). Neutral cases for both the MJO and SPV are categorized when the magnitude of the corresponding index (OMI or NAM_{100}) is less than 1σ. In order to increase the sample size for MJO composites, we have chosen to group MJO events into two main groups: (1) MJO Phases 2 and 3, associated with active (suppressed) convection over the Central-Eastern Indian Ocean and the Maritime Continent (the Pacific and Western Indian Oceans), and (2) MJO Phases 7 and 8, associated with active (suppressed) convection over the Dateline and Western Pacific (the Indian Ocean and Maritime Continent; e.g., Wheeler & Hendon, 2004; Zhang, 2005). Using the combined phases of the MJO (Phases 2 and 3, and 7 and 8) is also motivated by the results from L'Heureux and Higgins (2008), which show a relationship between the MJO and the Arctic oscillation during these phases. However, other studies have shown that the individual phases may produce different teleconnections that could be masked by combining the phases together in the compositing analysis (e.g., Tseng et al., 2018, 2018). The trade-off between the very small sample sizes of individual phase composites and the potential mix of teleconnections motivated us to keep with our phase groupings, though we consider the latter in our interpretation of the results.

Considering the above definitions, we now define specific criteria for our composite analyses. First, we will consider single-type events—that is, the composites oftentimes seen in the climate literature and used for operational S2S forecasting. The definitions are as follows:

- An MJO X + neutral SPV event is defined when the MJO amplitude exceeds 1σ and is in phase X, but the SPV is in a neutral state.

Table 1
Number of Events for Each Composite Category Used in This Study

	Neutral SPV	Weak SPV	Strong SPV
Neutral MJO		37	43
MJO Phase 2 and 3	68	23	21
MJO Phase 7 and 8	69	18	18

Note. SPV = stratospheric polar vortex; MJO = Madden-Julian oscillation.

- A strong SPV + neutral MJO event is defined when $NAM_{100} \geq 1\sigma$ but the MJO amplitude is neutral.
- A weak SPV + neutral MJO event is defined when $NAM_{100} \leq -1\sigma$, but the MJO amplitude is neutral.

Importantly, note that these single-type events consider that the other mode is neutral. This additional criterion is done so as to minimize any potential impacts that the SPV or MJO will have on the resulting composited fields.

Finally, our central hypothesis about the joint influence of the MJO and SPV will be tested with results from four conditional composite categories. These composites are denoted by the following nomenclature:

- MJO Phases 2 and 3 + weak SPV
- MJO Phases 2 and 3 + strong SPV
- MJO Phases 7 and 8 + weak SPV
- MJO Phases 7 and 8 + strong SPV

For all composites, the start date of the event (i.e., Day 0) is when the amplitude of the MJO, while in one of the two phase groups, exceeds 1σ and remains above this threshold for the next 3 days. These criteria also require the MJO to remain in the same phase for three consecutive days. Similar criteria are used for SPV events, but the amplitude of the event must exceed the threshold for five consecutive days. These minimum thresholds for days the indices must exceed a particular amplitude are implemented so as to (a) avoid single-day high-amplitude events and (b) ensure that either mode has sufficient time to impact NH extratropical weather patterns. These criteria for categorizing events are used for both single-type and joint composites. The start date for all events defined when the MJO fits the prescribed criteria and occurs during one of the three (weak, strong, or neutral) SPV event types. Table 1 displays the number of events for each of the composite categories. As seen, there are a larger number of MJO-only events compared to the SPV-only events. Also, there is a greater number of MJO Phases 2 and 3 than MJO Phases 7 and 8 events, including for the conditional categories. Although the number of events per category varies, even the smallest number of samples is sufficient to draw meaningful conclusions from this work.

For this study, we examine geophysical variables primarily with lags +10 to +14 days after the start date of the event. This 5-day average represents the time just into the subseasonal range, while it is beyond and acts to filter out synoptic timescale variability. Some variables (e.g., U) are also examined at longer lags (e.g., out to Days ±30; section 4.2) to illustrate other robust features of the circulation, particularly in the stratosphere. One caveat in our categorization scheme for these events involves the propagation speed of the MJO. That is, during the 14-days examined for the composites, the MJO could move into a new phase (e.g., from Phases 3 to 4). However, for the purposes of this study, we consider the phase of the MJO on Day 0 only for categorizing the single and joint composites.

Statistical significance of the composites is assessed using a two-tailed bootstrapping of $N = 5{,}000$ samples with replacement. That is, random start days of events are first selected, which are then used to find the corresponding +10- to 14-day composites. This process is then repeated 5,000 times to form a distribution from which the desired confidence interval (i.e., $p<0.05$) is found. For spatial correlation analysis (i.e., Figure 2), we use a slightly different technique. In this case, we generate 5,000 pairs of synthetic height anomaly maps for a given region (with similar latitude and longitude constraints) and correlate these pairs of maps. Our spatial correlation is then compared to the distribution of the 5,000 synthetic correlations to find its significance (i.e., $p<0.05$).

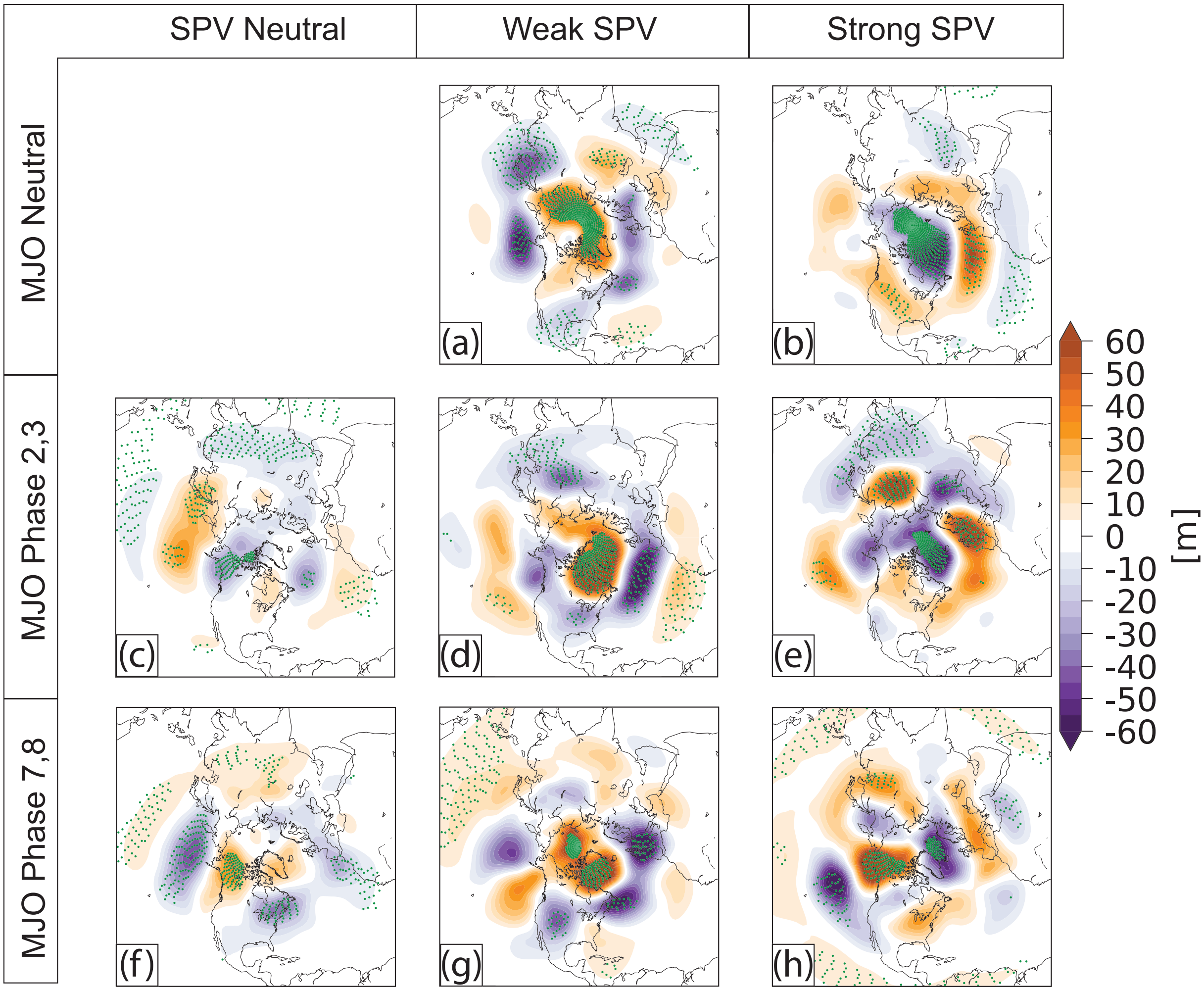

Figure 1. Days +10 to +14 averaged composites of October–March 500-hPa geopotential height anomalies (m) the eight MJO/SPV composite categories discussed in this study: (a) weak SPV + neutral MJO, (b) strong SPV + neutral MJO, (c) MJO Phases 2 and 3 + neutral SPV, (d) MJO Phases 2 and 3 + weak SPV, (e) MJO Phases 2 and 3 + strong SPV, (f) MJO Phases 7 and 8 + neutral SPV, (g) MJO Phases 7 and 8 + weak SPV, and (h) MJO Phases 7 and 8 + strong SPV. Green stippling indicates composite anomalies are significant at the p<0.05 level. SPV = stratospheric polar vortex; MJO = Madden-Julian oscillation.

3. Composite Analyses of the MJO and the SPV

3.1. The 500-hPa GPH Anomaly Composites

We begin our analysis by examining the midtropospheric flow pattern for the different composite categories. Looking at the neutral case composites first (Figure 1), we find familiar patterns of 500-hPa GPH anomalies as described in previous studies. For example, both the weak SPV + neutral MJO (Figure 1a) and strong SPV + neutral MJO (Figure 1b) cases reproduce the characteristic negative and positive tropospheric NAM structure, with opposite-signed height anomalies in the Arctic and the NH midlatitudes (e.g., Thompson & Wallace, 1998, 2000). Both MJOs 2 and 3 + neutral SPV (Figure 1c) and MJOs 7 and 8 + neutral SPV composite means (Figure 1f) illustrate a Rossby wave train emanating out of the Pacific and traveling along a great circle into western North America and then into the North Atlantic (e.g., Ferranti et al., 1990; Hoskins & Karoly, 1981; Mori & Watanabe, 2008; Moore et al., 2010). The negative (positive) NAM/NAO signature typically seen during MJO Phases 2 and 3 (7 and 8) events are also reproduced in these composites (e.g., Cassou, 2008; L'Heureux & Higgins, 2008; Lin et al., 2009).

Next, we consider the statistical significance of the anomalies in these neutral composite cases (i.e., green stippling in Figure 1). For the Weak SPV + neutral MJO events (Figure 1a), statistical significance in the composite signal (p<0.05) resides primarily across the Arctic, parts of Asia, and the North Pacific. Signals for troughing in the Eastern United States and North Atlantic feature some significance though not widespread, illustrating variability with different weak vortex regimes. For the strong SPV + neutral MJO composite (Figure 1b), statistically significant anomalies are prevalent throughout the Arctic and into the North Atlantic sector. In both the MJOs 2 and 3, and 7 and 8 + neutral SPV composite categories (Figures 1c and 1f), the North Pacific wave train signature is statistically significant. This significance extends into parts of North America, parts of central Asia, and the North Atlantic, especially for the MJO Phases 2 and 3 + neutral SPV case (Figure 1c). Because the MJO may interact with tropospheric weather patterns differently as the extratropical NH background state changes during the 6-month period examined, we split cases in our MJO + neutral SPV categories into those that occurred early (October through December) and late (January through March) in the extended boreal cold season and recomputed the corresponding composite-mean plots. The resulting composite patterns (not shown) are similar to the composite-mean patterns shown in Figure 1, thus reinforcing our findings.

Having verified our compositing technique works for the single-type cases, we next explore the conditional MJO-SPV categories. In the MJO Phases 2 and 3 + weak SPV composite mean (Figure 1d), ridging typically over the northwest Pacific (as seen in Figure 1c) shifts eastward toward western North America with troughing seen across Alaska. In the Atlantic, conditions resemble a negative NAO signature typical of weak SPV regimes (Figure 1a) but stronger in magnitude. A similar story emerges for the MJO Phases 2 and 3 + strong SPV composite-mean (Figure 1e)—that is, the Pacific sector resembles more of the MJO Phases 2 and 3 signature (Figure 1c), while the Atlantic sector captures the downward influence of the strong SPV via a positive NAO signature (Figure 1b). This central theme will repeat in subsequent analyses and presents the first major result of this study. That is, for the conditional composite cases, the MJO influences circulation anomalies across the North Pacific and western North America primarily, while the SPV has a closer association with tropospheric circulation anomalies in the Atlantic/Europe.

For the MJO Phases 7 and 8 + weak SPV composite mean (Figure 1g), an east-west height dipole is found in the North Pacific, while constructive interference between the two modes occurs over the Arctic and European regions. This constructive interference manifests via the negative NAM pattern throughout the midlatitudes, particularly across the Atlantic and Europe. The exception is North America, where weak ridging exists in the southeastern United States and over the Caribbean. The characteristic trough over eastern North America during weak SPV episodes (Figure 1a) appears shifted northwestward, generating statistically significant negative height anomalies across the western United States (Figure 1g). Indeed, the pattern resembles more of the negative phase of the PNA pattern in the MJO Phases 7 and 8 + weak SPV composite mean. By contrast, Figure 1h shows destructive interference between the MJO Phases 7 and 8 and SPV composite patterns. Only the Atlantic and European height anomalies (i.e., a positive NAO-like feature) are maintained and remain statistically significant when compared to the strong SPV + neutral MJO composite mean in Figure 1b (e.g., Figure 1h, green stippling). Elsewhere in the NH midlatitudes, the annular pattern disappears and is replaced by an overall Wave 4 or 5 structure (Figure 1h), though the North Pacific meridional dipole remains intact albeit shifted with respect to the MJOs 7 and 8 + neutral SPV composite (Figure 1f).

To objectively identify how the MJO and the SPV work to interfere with one another, spatial correlation coefficients are computed for five different regions. These regions included the whole NH, the North Pacific (20°–60° N, 150° E to 140° W), North America (20°–60° N, 60° to 120° W), the North Atlantic (20°–75° N, 60° W to 20° E), and Eurasia (20°–75° N, 30°–130° E). Throughout the 500-hPa GPH composites, we speculated that the MJOs 7 and 8 + weak SPV would have strong constructive interference with both the MJOs 7 and 8 + neutral SPV and the weak SPV + neutral MJO composites. Indeed, as indicated in Figure 2, the MJOs 7 and 8 + weak SPV composite mean 500-hPa GPH field exhibits statistically significant ($p<0.05$) positive correlations with the weak SPV + neutral MJO composite-mean pattern over the NH, North America, the North Atlantic, and Eurasia. When comparing this joint composite to the MJOs 7 and 8 + neutral SPV composite mean, all sectors except Eurasia have significant positive pattern correlations. Focusing on the MJOs 7 and 8 + strong SPV composite mean, a different pattern is found in the spatial correlations. Comparing the MJOs 7 and 8 + strong SPV to the MJOs 7 and 8 + neutral composite mean, the patterns across the whole NH, the North Pacific, and Eurasia are positively correlated and statistically significant, albeit small in value. Over North America and the North Atlantic, however, the pattern correlations are significantly negative, showing strong destructive interference. When comparing the strong SPV + neutral MJO and MJOs 7 and 8 + strong SPV composite-mean patterns, statistically significant positive correlations exist only over the NH and the North Atlantic (Figure 2).

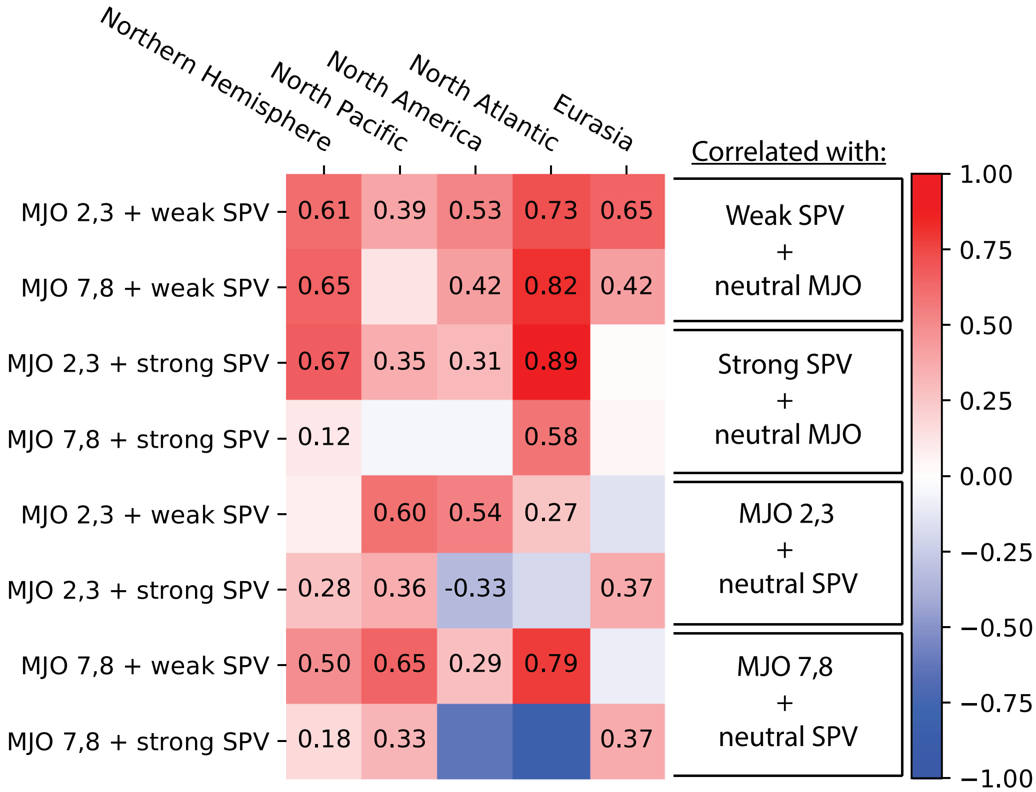

Figure 2. Spatial correlation coefficients of MJO and SPV neutral composites against the various combined MJO + SPV events in Figure 1 over the entire Northern Hemisphere, the North Pacific (20°–60° N, 150° E to 140° W), North America (20°–60° N, 60°–120° W), the North Atlantic (20°–75° N, 60° W to 20° E), and Eurasia (20°–75° N, 30°–130° E). Only correlation coefficients significant at the $p<0.05$ level are explicitly shown. SPV = stratospheric polar vortex; MJO = Madden-Julian oscillation.

3.2. The 250-hPa U Anomaly Composites

Having examined the midtropospheric wave patterns via 500-hPa GPH anomalies, we next turn to examine composite differences in the jet structure, as represented by 250-hPa U anomalies (Figure 3). Examining the upper-tropospheric winds allows us to more explicitly examine storm tracks and also potential changes in both the subtropical and polar jet streams. The jet structure for the weak (strong) SPV + neutral MJO composite category shows anomalies that are characteristic of the negative (positive) phase of the tropospheric NAM, that is, a weakening (strengthening) of upper-tropospheric zonal winds at higher latitudes, particularly over North America, the Atlantic, and Europe (Figures 3a and 3b). MJO events occurring during neutral SPV times also influence the jet stream but in different regions. The MJO Phases 2 and 3 + neutral SPV events (Figure 3c) accelerate the climatological westerlies (contours in all panels of Figure 3) over central Asia, or north of the enhanced convection in the Indian Ocean with negative zonal wind anomalies also present over the North Pacific basin, indicating a retracted Pacific jet (Moore et al., 2010; Zhou & Miller, 2005). Except for a region of statistically significant anomalies across the North Atlantic jet, there are no significant 250-hPa U wind anomalies across North America or Europe for the MJO Phases 2 and 3 + neutral SPV composite mean. By contrast, the MJO Phases 7 and 8 + neutral SPV composite mean (Figure 3f) exhibits an extended Asian-Pacific jet stream (e.g., Moore et al., 2010; Rui & Wang, 1990; Zhou & Miller, 2005), along with an acceleration of the polar jet off of eastern North America. Likewise, the jet stream appears to shift equatorward, to the north of the suppressed convection in the Indian Ocean.

The conditional composites for the 250-hPa U anomalies (Figures 3d, 3e, 3g, and 3h) are dynamically consistent with their 500-hPa GPH anomalies counterparts (Figures 1d, 1e, 1g, and 1h). Again, features characteristic of classic MJO composites reemerge in the Pacific sector, while those associated with the SPV/NAM appear in the Atlantic sector (i.e., positive or negative NAO conditions). Yet there are other important

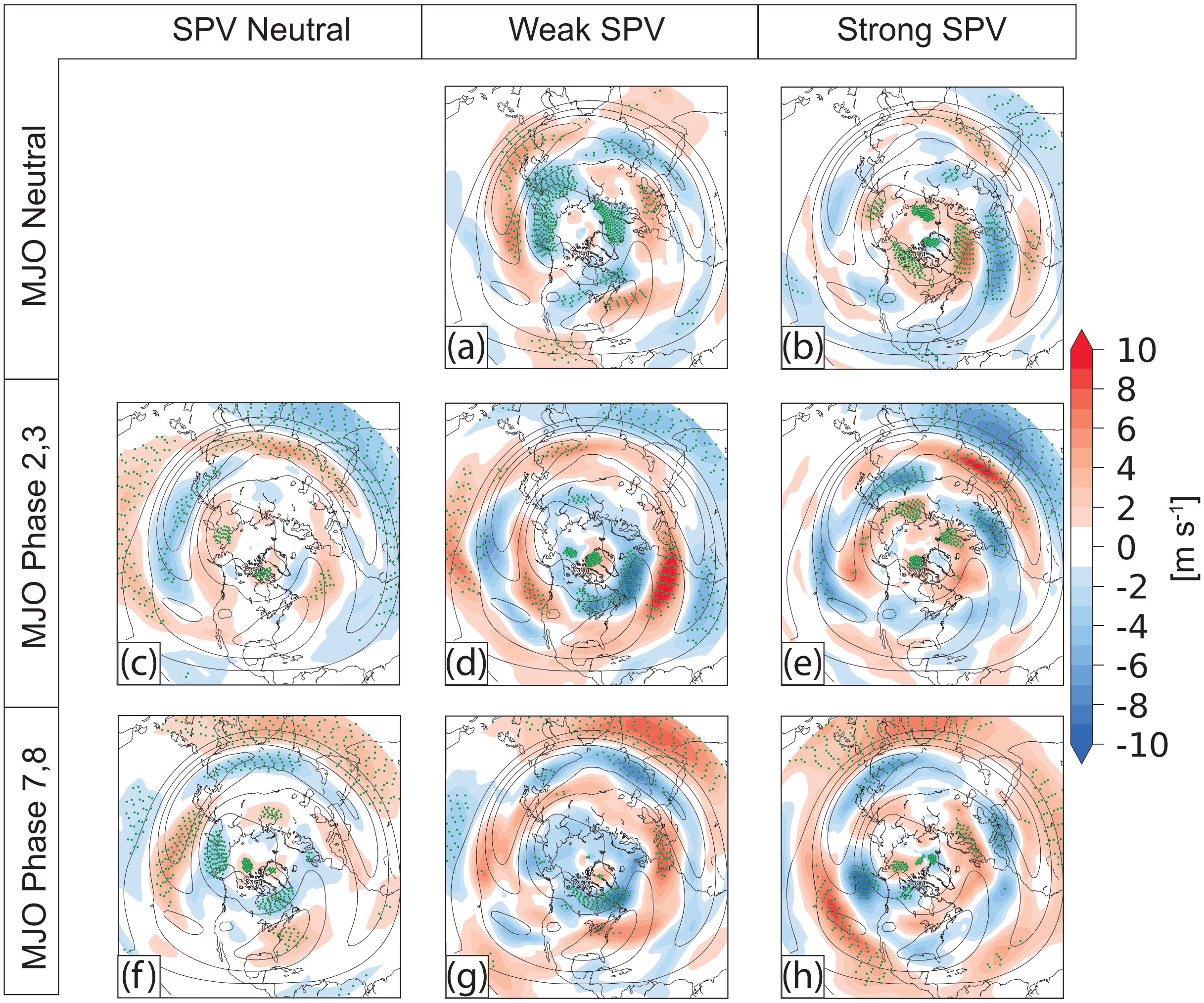

Figure 3. Shading and stippling: same as Figure 1 but for 250-hPa zonal wind (U) anomalies (m/s). Line contours: October–March climatological 250-hPa U (m/s). Contours from 10 to 40 meters per second every 10 m/s. SPV = stratospheric polar vortex; MJO = Madden-Julian oscillation.

findings from the U anomaly composites not seen in the 500-hPa GPH anomaly plots. For example, the MJO Phases 2 and 3 + weak SPV composite (Figure 1d) shows an intensified polar jet (and subsequently, storm track) over much of North America across to Europe, reinforcing the negative NAO regime in place Figure 1d). This enhanced jet off of eastern North America has some connections to anomalies extending back into the subtropical Pacific (although anomalies are not significant), indicating potentially an enhanced and more moisture-laden storm track because of connections to the subtropical Pacific. By contrast, for the MJO Phases 7 and 8 + weak SPV composite (Figure 1g), the eastern North America-Atlantic jet stream is displaced poleward compared to weak SPV + neutral MJO events (and poleward of the climatological jet stream in eastern North America; Figure 1g, line contours). Changes in the Atlantic jet are even less apparent during MJO Phases 2 and 3 + strong SPV cases when compared against the strong SPV + neutral MJO composite (Figure 3b). Moreover, the regional pattern exhibits considerably less statistical significance there (Figure 3e). MJO Phases 7 and 8 + weak SPV cases (Figure 3g) show large-scale constructive interference between the MJOs 7 and 8 + neutral SPV and Weak SPV + neutral MJO composites throughout the NH, while the conditional MJO Phases 7 and 8 + strong SPV composite mean (Figure 3h) displays destructive interference between the two modes throughout the Arctic and Europe with weak enhancement of the Pacific features seen with the MJO-neutral SPV composite (Figure 3f). As such, the conditional composites elude to differences in the jet stream/storm tracks that would be potentially missed if relying only on the single-index composites, especially for North America.

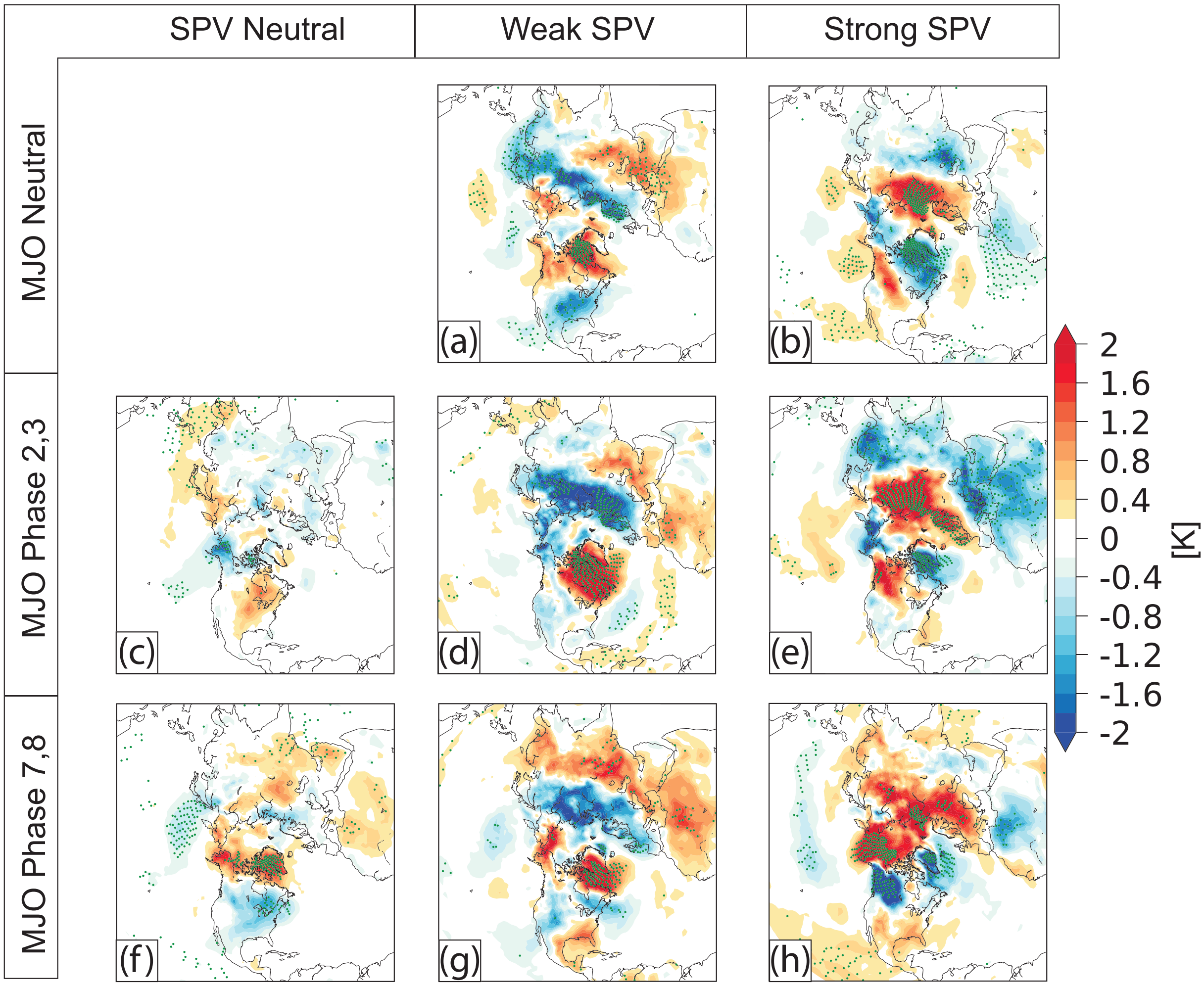

Figure 4. Same as Figure 1 but for surface air temperature anomalies (K).

3.3. SAT Anomaly Composites

While the 500-hPa GPH and 250-hPa U anomaly composites give insight into main circulation features associated with the different MJO/SPV cases, we next examine the SAT anomaly composites, a very common variable used for S2S operational forecasts, to highlight sensible weather impacts of the different cases at the surface (Figure 4). The SAT anomaly composite for the SPV + neutral MJO cases (Figures 4a and 4b) show warm (cold) anomalies in northern North America and Greenland and cold (warm) anomalies in northern Asia for weak (strong) SPV cases, consistent with previous studies (e.g., Thompson & Wallace, 2000, 2001; Waugh et al., 2017). The MJO + neutral SPV composites (Figures 4c and 4f) show weak (and mostly statistically insignificant) anomalies across Europe and large parts of Asia. Given its association with the positive (negative) tropospheric NAM, much of North America (outside of Alaska) experiences warmer (colder) than average conditions during MJO Phases 2 and 3 (Phases 7 and 8), though significance is poor for much of North America (Figures 4c and 4f; green stippling).

Turning to the joint composite categories, the case for which mode is preferred in the patterns of different regions becomes quite apparent. In all conditional cases, SAT anomalies across Europe and most of Asia almost entirely resemble the SAT anomalies we would expect if only considering the state of the SPV (e.g., compare the Eurasian SAT anomalies in Figures 4d and 4g with Figures 4a and Figures 4e and 4h with Figure 4b). As such, these conditional composites further emphasize that, out of the two climate modes considered for this study, the state of the SPV and its influence on the tropospheric NAM better represents resulting circulation patterns across most of Eurasia versus the MJO or the MJO + SPV conditional composites. This result differs slightly from the height composites as we only observe strong correlations of the MJO + weak SPV with the weak SPV + neutral MJO composites in this sector (Figure 2). However, a different story emerges for North America. Here, we see considerable variance between the conditional composites when compared to either of the single-index composites. For example, both the weak SPV + neutral MJO (Figure 4a) and the MJO Phases 7 and 8 + neutral SPV (Figure 4f) composites show the propensity for negative SAT anomalies across much of the eastern half of North America. However, for the MJO Phases 7 and 8 + weak SPV cases (Figure 4g), significant cold anomalies only appear across far northeastern North America, with almost no signal in central North America and even *warm* anomalies (though mostly insignificant) across the Southeast and Mid-Atlantic United States. Similarly, while MJO Phases 2 and 3 are typically regarded as yielding mild spells for much of United States and central Canada (Figure 4c; Zhou et al., 2012), the conditional composites suggest uncertainty to that warm signal (Figures 4d and 4e). These unique patterns in the conditional composites also hint to possible nonlinear interactions between the MJO and the SPV, which we address in a later section. Therefore, from a forecasting perspective, considering both the state of the SPV and the phase of the MJO may alter forecast rationale for winter SAT predictions across much of North America.

4. Stratosphere-Troposphere Dynamical Coupling Composites

4.1. EP-Flux Composites

So far, joint composites of several variables illustrate significantly different patterns across much of the NH for the different MJO/SPV categories, which lends confidence that the findings could be useful for forecasting applications. However, based on previous literature, convection associated with the MJO impacts both horizontal and vertical wave propagation into the tropical and NH extratropical stratosphere (e.g., Garfinkel et al., 2012; Weare, 2010). As such, there is the possibility that the MJO not only influences tropospheric weather patterns directly but also influences the SPV, which then exerts a downward influence on the tropospheric circulation. That possibility is a caveat of this study and discussed later. Instead, in this section, we will examine whether vertically propagating Rossby waves exhibit different characteristics depending on the various composite cases and subsequently how these different characteristics can influence dynamical NH extratropical stratosphere-troposphere variability.

Figure 5 presents the Day +10 to +14-averaged EP fluxes $\left(\vec{F}\right)$ and EP flux divergence $\left(\nabla\cdot\vec{F}\right)$ plotted for our MJO and SPV cases. $\vec{F}$ has two components: (a) the latitudinal component F_φ, which is proportional to the *negative* of horizontal momentum flux (i.e., $-\overline{u'v'}$), and (b) the vertical component F_p, which is proportional to meridional heat flux (i.e., $\overline{v'T'}$). Per the zonal-mean momentum equation, $\nabla\cdot\vec{F}$ affects the acceleration of the zonal-mean zonal wind. The SPV + neutral MJO cases (Figures 5a and 5b) agree with the results by Thompson et al. (2006), which show how a weak (strong) SPV can act to reorganize tropospheric eddies at middle-to-high latitudes in the troposphere to shift the overall mean polar jet stream equatorward (poleward) via anomalous momentum fluxes pumping westerly momentum equatorward (poleward) (Figures 5a and 5b, horizontal component of the EP flux vectors). By contrast, there are relatively small EP flux anomalies in the stratosphere during MJO Phases 2 and 3 + neutral SPV cases (Figure 5c). The lack of substantial flux anomalies in the stratosphere during MJO Phases 2 and 3 events carries over for the conditional composites associated with these phases as well (Figures 5d and 5e). Instead, enhanced poleward (equatorward) fluxes in the middle and upper troposphere (between about 30° and 60° N) appear during MJO Phases 2 and 3 + weak (strong) SPV, consistent with the findings from the corresponding SPV + neutral MJO composites (Figures 5a and 5b). Therefore, this analysis suggests that anomalous wave propagation associated with MJO Phases 2 and 3 events are more confined to the troposphere with minimal influence on the stratosphere. Taken another way, the observed influence that MJO Phases 2 and 3 alone has on the NAM/NAO could be primarily through a tropospheric pathway.

Results are different for events involving MJO Phases 7 and 8. For MJO Phases 7 and 8 + neutral SPV cases (Figure 5f), anomalous poleward and upward propagation of Rossby waves exist north of about 50° N, leading to anomalous EP flux convergence (i.e., wave breaking) in the extratropical NH stratosphere and thus deceleration of the polar night jet there. There is also EP flux convergence in the troposphere north of 60° N. In the MJO Phases 7 and 8 + weak SPV events (Figure 5g), similar patterns to that of the weak

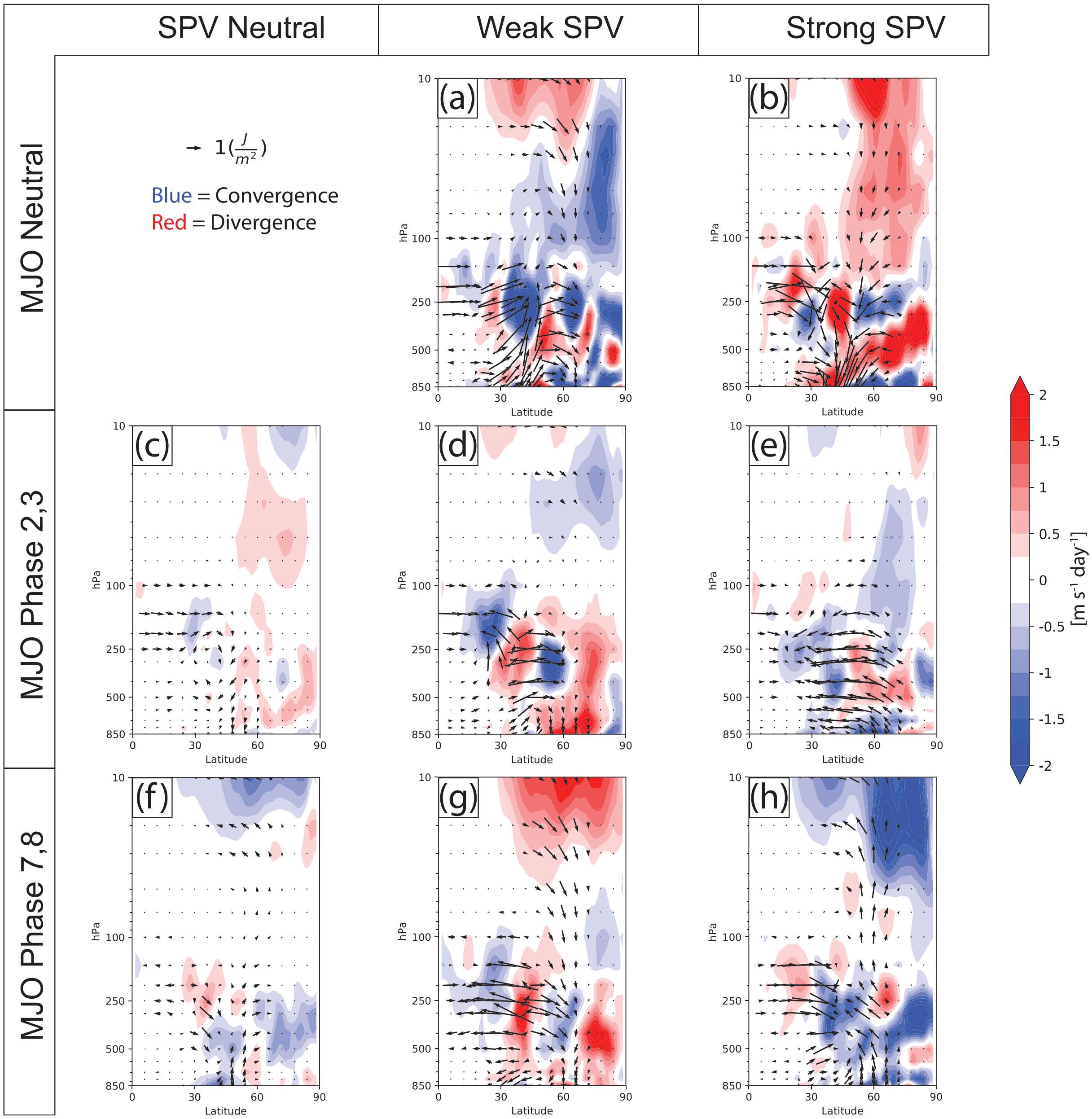

Figure 5. Day +10 to +14 averaged Eliassen-Palm (EP) flux (vectors, J/m^2) and flux divergence (shading, m·s^{-1}·day^{-1}) anomalies for the eight MJO/SPV composite categories discussed in this study: (a) weak SPV + neutral MJO, (b) strong SPV + neutral MJO, (c) MJO Phases 2 and 3 + neutral SPV, (d) MJO Phases 2 and 3 + weak SPV, (e) MJO Phases 2 and 3 + strong SPV, (f) MJO Phases 7 and 8 + neutral SPV, (g) MJO Phases 7 and 8 + weak SPV, and (h) MJO Phases 7 and 8 + strong SPV. EP-flux vectors scaled for plotting by $\rho r_E \cos\varphi\left(\frac{F_\varphi}{r_E s_\varphi}, \frac{F_p}{s_p}\right)$, where $\rho = \sqrt{\frac{1{,}000}{p}}$, p is pressure, φ is latitude, F_φ is the horizontal component of the EP flux vector, F_p is the vertical component of the flux, r_E is the radius of Earth, $s_\varphi=\pi$, and $s_p=1\times10^5$ Pa. EP-flux divergence (red shading) and convergence (blue shading) scaled by $(\rho r_E \cos\varphi)^{-1}$ (to make units of acceleration) and contoured every 0.25 m·s^{-1}·day^{-1} from −2 m·s^{-1}·day^{-1} to 2 m·s^{-1}·day^{-1}. Reference vector included. SPV = stratospheric polar vortex; MJO = Madden-Julian oscillation.

SPV + neutral MJO are visible, with a large region of anomalous downward EP flux and subsequent anomalous EP flux divergence in the stratosphere. Anomalous poleward wave propagation still appears in the troposphere from about 40°–60° N under these conditions, though the pattern of anomalous convergence/divergence is less distinct than the weak SPV composites (Figure 5a). Note that this EP flux pattern is different than that in Figure 5f, which shows upward wave flux anomalies in the troposphere and stratosphere poleward of about 45° N. The difference here apparently is due to the influence of the weak westerlies present in the stratosphere, which shield the vortex from vertically propagating wave

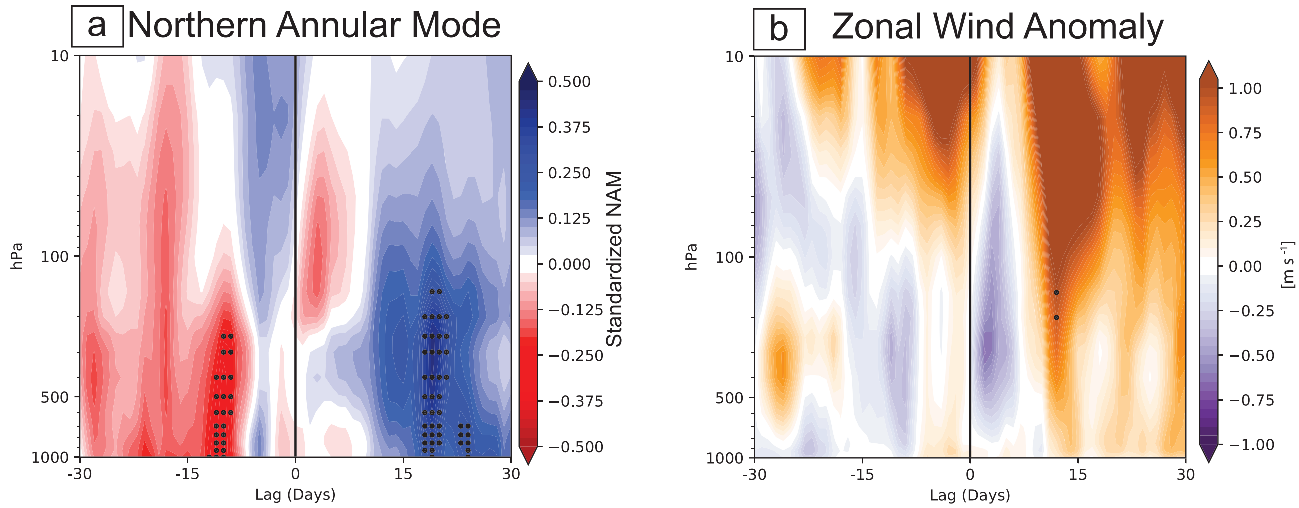

Figure 6. Pressure-time lag composites of the (a) standardized NAM index and (b) area-averaged (60° N to 80° N) zonal-mean zonal wind anomalies (m s^{-1}) for MJO Phase 2 and 3 + neutral SPV events. Day 0 represents the start date of the MJO event (black vertical line in both plots). Negative (positive) lags indicate the variable leads (lags) the start of the MJO event. Black stippling indicates composite values significant at the $p<0.05$ level. NAM = Northern Annular Mode; SPV = stratospheric polar vortex; MJO = Madden-Julian oscillation.

fluxes and thus change the relationship of the MJO Phases 7 and 8 with the stratospheric circulation. The patterns of the MJO Phases 7 and 8 + strong SPV (Figure 5h) are essentially opposite to those observed in Figure 5b, with anomalous convergence in the polar stratosphere leading to a breakdown/weakening of the SPV. This pattern is consistent with the findings of, for example, Garfinkel et al., 2012 (2012, 2014) and Schwartz and Garfinkel (2017). The contrast between Figures 5b and 5h suggests that the changes in amplitude of the tropospheric wave activity initiated by the MJO Phases 7 and 8 events may alter the state of the stratosphere via enhancing upward wave fluxes. Subsequently, stratospheric anomalies can then descend with time later to influence the tropospheric circulation (e.g., Baldwin & Dunkerton, 2001). As such, the MJO Phases 7 and 8 relationship with the tropospheric NAM/NAO may act both with a tropospheric *and* a (delayed—i.e., beyond our composite window) stratospheric pathway.

4.2. Lag Composites of Stratosphere-Troposphere Coupling Metrics for MJO Events

Analysis of the EP fluxes for the different MJO-SPV cases suggest that the MJO can interact with the NAM/NAO via both tropospheric and stratospheric pathways. In this study, we seek to address whether the MJO and the SPV can work independently from one another to influence NH winter weather patterns or if the MJO acts to influence the SPV. This distinction would determine if the composites presented thus far have been influenced by both of the modes separately or if they are an artifact of the MJO working through the SPV. In particular, we will explore the MJO + neutral SPV composites to see if the MJO first interacts with the stratosphere to influence its state and then subsequently the SPV influences the tropospheric circulation pattern via downward control.

We first analyze how lag composites of the NAM index throughout the troposphere and the stratosphere change for MJO + neutral SPV events (Figures 6a and 7a). In all lagged composites, Day 0 represents the start day of the event. For the MJO Phases 2 and 3 + neutral SPV composite (Figure 6a), while negative NAM conditions exist in the troposphere during negative lags (and are significant especially around Days −12 to −8), the trend during positive lags is toward a positive NAM state, with the largest positive NAM anomalies in the troposphere, extending upward into the stratosphere simultaneously at later lags. This evolution is different from the MJO Phases 7 and 8 + neutral SPV composite cases (Figure 7a), where the tropospheric NAM becomes significantly negative 5–10 days after the MJO event start date. The stratospheric NAM index turns anomalously negative after the tropospheric NAM has reached its peak negative value (see green box in Figure 7a). This evolution makes sense from the wave propagation analyzed in Figure 5f, where the MJO Phases 7 and 8 events change the tropospheric Rossby wave sources, which then propagate vertically and converge in the stratosphere, weakening the vortex (i.e., a negative NAM state).

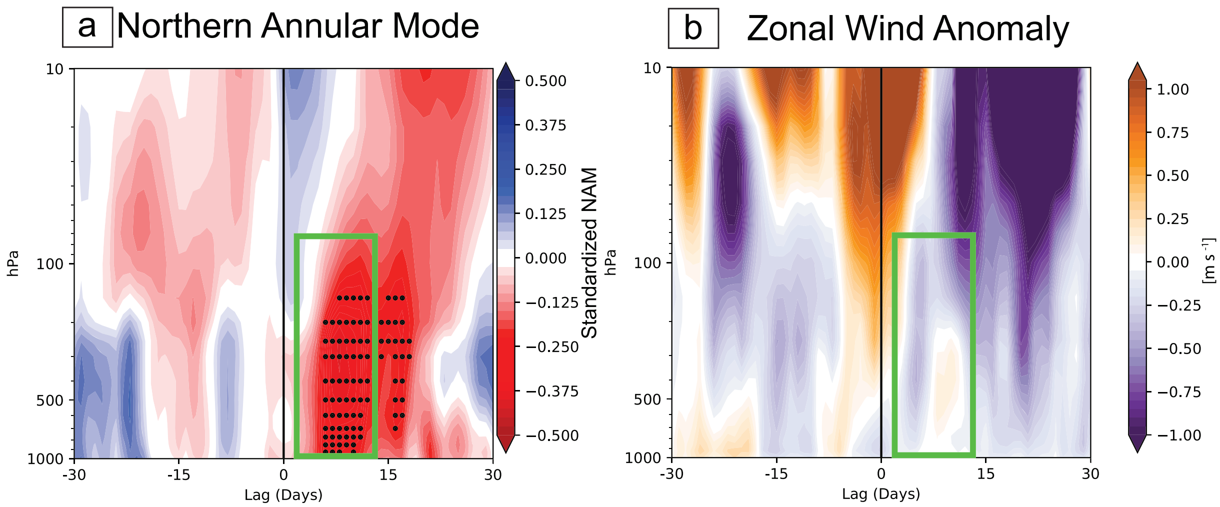

Figure 7. As in Figure 6, but for MJO Phases 7 and 8 + neutral SPV. Green box shows the evolution of the standardized NAM and zonal-mean zonal wind values as they change from the troposphere to the stratosphere. NAM = Northern Annular Mode; SPV = stratospheric polar vortex; MJO = Madden-Julian oscillation.

Figures 6b and 7b examine more explicitly the changes in the SPV potentially influenced by the MJO. During MJO Phases 2 and 3 + neutral SPV events, the SPV features positive zonal-mean U anomalies for both positive and negative lags, with the largest composite anomalies during Days −15 to 0 and Days +15 to +25. There is some evidence of zonal-mean U anomalies significantly descending with time from the stratosphere

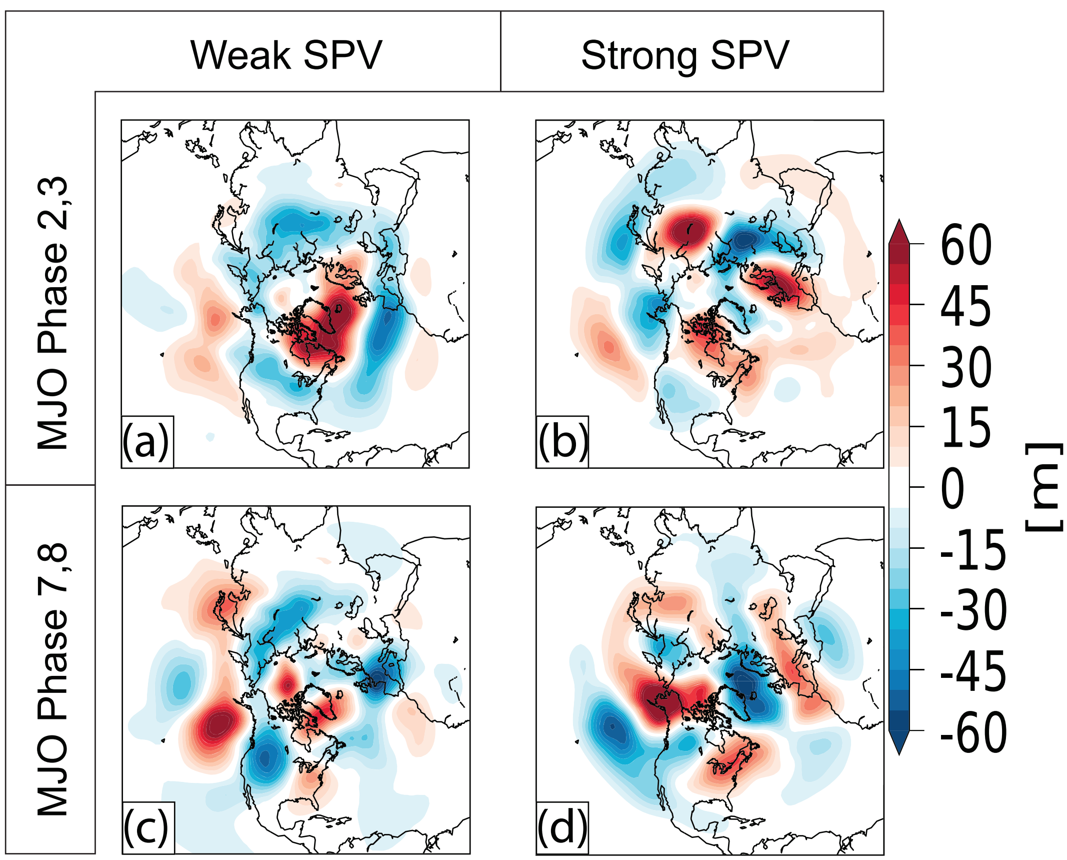

Figure 8. Residual 500-hPa geopotential height anomalies (m) for the combined MJO-SPV categories investigated in this study derived from the linear regression model (see text) and compositing analysis from Figure 1 (i.e., composite-regression). SPV = stratospheric polar vortex; MJO = Madden-Julian oscillation.

to the troposphere, but mostly, the anomalies occur almost simultaneously throughout the atmospheric column. It is not until late in the time series (greater than Day +20) that we see any indication of downward propagation of positive zonal-mean U anomalies in the stratosphere enter into the lower troposphere (Figure 6b). In Figure 7b, we see a clear reversal of the strength of the SPV above 100 hPa during positive lags with positive anomalies at Day 0 at 10 hPa turning negative by Day +10 and remaining negative through Day +30. In the troposphere, however, zonal-mean U decelerates, associated with a decrease in tropospheric NAM values (Figure 7a), before the SPV weakens (shown in green box on Figure 7). Signs of downward propagation of negative zonal-mean U anomalies appear after Day +15, suggesting that at longer leads, the MJO influence on the stratosphere might then feed back onto the tropospheric circulation. In both zonal-mean U composites, however, the anomalies are mostly statistically insignificant, which makes drawing more definitive conclusions difficult.

Taken together, the results here suggest that for our window of composite analysis (+10–14 days after event), the MJO's influence in either case first acts to alter the tropospheric circulation. This means that the findings from our composites in section 3 are the result of each mode (the MJO and the SPV) acting in concert on the tropospheric circulation and not necessarily the MJO acting through the stratosphere first. The stratospheric pathway may be more important at later lags, but this analysis is reserved for future work.

5. Discussion and Conclusions

The analyses in this work produced the following key findings, which directly address the guiding research questions from section 1:

1. Between the MJO and the SPV, the MJO influences most strongly tropospheric circulation patterns across the North Pacific and parts of western North America, while variability in the SPV strongly influences patterns over the North Atlantic and Europe (Figures 1-4).
2. For the geophysical variables studied (i.e., 500-hPa GPH, jet stream level winds, and SAT anomalies), constructive interference between the influences of the MJO and the SPV occurs during MJO Phases 2 and 3 + strong SPV and MJO Phases 7 and 8 + weak SPV episodes. Destructive interference between the influences of the two modes occurs for MJO Phases 2 and 3 + weak SPV and MJO Phases 7 and 8 + strong SPV episodes. These constructive and destructive influences are mostly seen in eastern North America and into the North Atlantic. These conclusions were also quantified via spatial correlations for the GPH composites (Figure 2). Our findings also agree with the documented linkages between the MJO and the tropospheric NAM/NAO (e.g., Cassou, 2008; Lin et al., 2009; L'Heureux & Higgins, 2008). The MJO Phases 7 and 8 + strong SPV composites show the strongest destructive interference relative to the MJO Phases 7 and 8 + neutral SPV composite (Figure 2).
3. MJO Phases 2 and 3 + neutral SPV events are associated with a strengthening of the SPV, while MJO Phases 7 and 8 + neutral SPV events are associated with a weakening of the SPV. Although the MJO interacts with the NAM throughout the troposphere and stratosphere, the strongest signal remains in the troposphere (Figures 6 and 7), suggesting that the MJO acts on the extratropical flow pattern primarily through a tropospheric pathway but could later impact the tropospheric circulation at longer lead times indirectly through its impacts on the SPV (e.g., Figure 7).

The overall implications of our findings are twofold. First, from an operational S2S forecasting perspective, understanding which areas are more related to the MJO versus the SPV can make a difference in making skillful wintertime forecasts. For example, forecasters in Europe may want to pay particular attention to the state of the SPV for their long-range forecasts rather than the current phase of the MJO. Though dynamical seasonal forecasting models include both of these modes in their forecasts, the fidelity with which models capture the evolution of and teleconnections of these modes differs, especially when it comes to stratosphere-troposphere coupling dynamics. Coupled models have a difficult time capturing the downward propagation of stratospheric anomalies into the troposphere, limiting the influence of the simulated stratosphere on tropospheric winter weather patterns (e.g., Furtado et al., 2015; Karpechko et al., 2017; Riddle et al., 2013). There are also opportunities for improved forecasts for North America, especially for the eastern half of the continent. This region showed divergent signals between our conditional and the single-index composites. For example, the shift toward a more negative PNA-like pattern across North America during MJO Phases 7 and 8 + weak SPV (Figure 1g) versus the more classic eastern North American trough seen during weak SPV + neutral MJO

(Figure 1a) and MJO Phases 7and 8 + neutral SPV (Figure 1f) cases has large implications for sensible weather conditions that would be missed if forecasters relied on only one of the two modes. Note, however, that our joint composites are limited in total samples versus the single-index composites. This difference in sample size is expected and warrants caution when interpreting our composite results.

The second key implication of this work lies in characterizing the dynamical interplay between the MJO and the SPV. We explored some of these aspects via wave propagation and stratosphere-troposphere dynamical coupling metrics (section 4). Here, evidence suggests that both MJO Phases 2 and 3 and Phases 7 and 8 act on the tropospheric circulation directly first, inducing changes in the polar jet stream/the tropospheric NAM. Any changes in the stratosphere appear secondary but may lead to persistence in the tropospheric signal at longer lags. This extended subseasonal predictability is important to explore further—that is, while extended predictability of the tropospheric NAM classically has thought to originate from changes in the SPV, this could indeed also be conditional on how other modes like the MJO precondition the troposphere. Note, for example, that during MJO Phases 2 and 3 + neutral SPV events (Figure 6), positive NAM conditions induced in the troposphere (Figure 6a) coincide with a strengthening of stratospheric winds (Figure 6b), which persist out to Day +30. More on this long-range persistence needs to be examined. Finally, while we considered the influence of the MJO onto the SPV, there is also the possibility that the state of the SPV can, in turn, influence tropical convection patterns and the MJO itself. Some studies (e.g., Gómez-Escolar et al., 2014; Kodera, 2006) suggest that weak SPV episodes have connections with tropical tropopause temperatures, which could indirectly alter tropical convection patterns. More work on this avenue of connections between the polar stratosphere and tropical climate variability needs to be pursued.

The composite technique used in this study was chosen to address potential nonlinearities in the combined MJO/SPV cases. However, given some of the similarities in the single-index versus joint composites, we need to also ask, how much of the signal in the conditional composites is merely a linear combination of the two single-mode composites? To answer this question, we constructed a linear regression model using the composite patterns of the SPV + neutral MJO and the MJO + neutral SPV to predict 500-hPa GPH anomalies with a lag of +10–14 days. The full form of the linear regression model is

$$\mathrm{GPH}_{500}(x) = \alpha \times \mathrm{COMP}_{\mathrm{SPV+neutral\ MJO}}(x) + \beta \times \mathrm{COMP}_{\mathrm{MJO+neutral\ SPV}}(x) + \gamma, \tag{1}$$

where x represents space; $\mathrm{COMP}_{\mathrm{SPV\text{-}Neutral\ MJO}}$ and $\mathrm{COMP}_{\mathrm{MJO\text{-}Neutral\ SPV}}$ represent the SPV + neutral MJO and MJO + neutral SPV composites found in Figure 1, respectively; and α, β, and γ are coefficients found through least squares fitting. Figure 8 shows the residual between the linear regression model and the composite results (i.e., composite-regression) evaluated for the same events included in the joint MJO/SPV composites in Figure 1. In the limit that the signals seen in the composites were purely linear combinations of the MJO and the SPV influences, the difference plots in Figure 8 would be blank/all zero. Since these plots show some structure, we can infer firstly that the collective influence of the MJO and the SPV is not simply linear. Indeed, we see large differences in the linear regression model and the composites across the entire NH. Some regions, such as the Pacific-North American and Atlantic-European sectors, exhibit some of the strongest differences. We conclude that the influence of the MJO and SPV on the tropospheric circulation is not a simple linear combination of the two modes of variability. As such, composite analysis conducted in this study is more applicable for analyzing these events versus linear regression because of its ability to capture both linear and nonlinear processes.

Additional work on this topic will involve examining our findings in dynamical model forecasts of these particular events, along with evaluation of model-based events themselves. Multimodel suites like the International S2S Prediction Project Database (Vitart et al., 2017) can be used to test our hypotheses further and even examine how, for example, models with and without realistic NH SPV variability recover the MJO-SPV joint composites. Moreover, using these methods within specific case studies for the different composite categories and in different regions of the NH would show how they perform different when applied to specific events. This further work would aid in the expansion of understanding and improve the predictability of S2S weather and climate patterns related to the MJO and SPV variability.

Acknowledgments
This research has been conducted as part of the National Oceanic and Atmospheric Administration (NOAA) Model, Analysis, Prediction, and Projections (MAPP) S2S Prediction Task Force and is supported by NOAA Oceanic and Atmospheric Research (OAR) Climate Program Office (CPO) Grant NA16OAR4310075. The ERA-Interim data used for this work were produced by ECMWF and is freely accessible (upon registration) via their site (https://www.ecmwf.int/en/forecasts/datasets/archive-datasets/reanalysis-datasets/era-interim). The OMI is also available via the NOAA ESRL website (https://www.esrl.noaa.gov/psd/mjo/mjoindex/). The authors would like to thank Elizabeth Barnes, Laura Ciasto, and Michelle L'Heureux for advice and comments on some of the analysis and results presented in this paper. The authors would also like to thank three anonymous reviewers for their constructive comments and suggestions, which ultimately improved the quality of the manuscript.

References

Baldwin, M. P., & Dunkerton, T. J. (1999). Propagation of the Arctic Oscillation from the stratosphere to the troposphere. *Journal of Geophysical Research*, *104*, 30,937–30,946. https://doi.org/10.1029/1999JD900445

Baldwin, M. P., & Dunkerton, T. J. (2001). Stratospheric harbingers of anomalous weather regimes. *Science*, *294*, 581–584. https://doi.org/10.1126/science.1063315

Baldwin, M. P., Stephenson, D. B., Thompson, D. W. J., Dunkerton, T. J., Charlton, A. J., & O"Neill, A.(2003). Stratospheric memory and skill of extended-range weather forecasts. *Science*, *301*, 636–640.

Barnston, A. G., & Livezey, R. E. (1987). Classification, seasonality and persistence of low-frequency atmospheric circulation patterns. *Monthly Weather Review*, *115*, 1083–1126. https://doi.org/10.1175/1520-0493(1987)115<1083:CSAPOL>2.0.CO;2

Cassou, C. (2008). Intraseasonal interaction between the Madden-Julian Oscillation and the North Atlantic Oscillation. *Nature*, *455*, 523–527. https://doi.org/10.1038/nature07286

Charney, J. G., & Drazin, P. G. (1961). Propagation of planetary-scale disturbances from the lower into the upper atmosphere. *Journal of Geophysical Research*, *66*, 83–109. https://doi.org/10.1029/JZ066i001p00083

Dee, D. P., Uppala, S. M., Simmons, A. J., Berrisford, P., Poli, P., Kobayashi, S., et al. (2011). The ERA-interim reanalysis: Configuration and performance of the data assimilation system. *Quarterly Journal of the Royal Meteorological Society*, *137*, 553–597. https://doi.org/10.1002/qj.828

Edmon, H. J., Hoskins, B. J., & McIntyre, M. E. (1980). Eliassen-Palm cross sections for the troposphere. *Journal of the Atmospheric Sciences*, *37*, 2600–2616.

Ferranti, L., Palmer, T. N., Molteni, F., & Klinker, E. (1990). Tropical-extratropical interaction associated with the 30–60 day oscillation and its impact on medium and extended range prediction. *Journal of the Atmospheric Sciences*, *47*, 2177–2199.

Frederiksen, J. S., & Lin, H. (2013). Tropical–extratropical interactions of intraseasonal oscillations. *Journal of the Atmospheric Sciences*, *70*, 3180–3197. https://doi.org/10.1175/JAS-D-12-0302.1

Furtado, J. C., Cohen, J. L., Riddle, E. E., Butler, A. H., & Kumar, A (2015). Eurasian snow cover variability and links to winter climate in the CMIP5 models. *Climate Dynamics*, *45*, 2591–2605. https://doi.org/10.1007/s00382-015-2494-4

Garfinkel, C. I., Benedict, J. J., & Maloney, E. D. (2014). Impact of the MJO on the boreal winter extratropical circulation. *Geophysical Research Letters*, *41*, 6055–6062. https://doi.org/10.1002/2014GL061094

Garfinkel, C. I., Feldstein, S. B., Waugh, D. W., Yoo, C., & Lee, S. (2012). Observed connection between stratospheric sudden warmings and the Madden-Julian Oscillation. *Geophysical Research Letters*, *39*, L18807. https://doi.org/10.1029/2012GL053144

Gómez-Escolar, M., Calvo, N., Barriopedro, D., & Fueglistaler, S. (2014). Tropical response to stratospheric sudden warmings and its modulation by the QBO. *Journal of Geophysical Research: Atmospheres*, *119*, 7382–7395. https://doi.org/10.1002/2013JD020560

Haynes, P. H., Marks, C. J., McIntyre, M. E., Shepherd, T. G., & Shine, K. P. (1991). On the "downward control" of extratropical diabatic circulations by eddy-induced mean zonal forces. *Journal of the Atmospheric Sciences*, *48*, 651–678.

Henderson, S., Maloney, E., & Barnes, E. A. (2016). The influence of the Madden-Julian oscillation on Northern Hemisphere winter blocking. *Journal of Climate*, *29*, 4597–4616. https://doi.org/10.1175/JCLI-D-15-0502.1

Hendon, H. H., Wheeler, M. C., & Zhang, C. (2007). Seasonal dependence of the MJO–ENSO relationship. *Journal of Climate*, *20*, 531–543.

Hoskins, B. J., & Karoly, D. J. (1981). The steady linear response of a spherical atmosphere to thermal and orographic forcing. *Journal of the Atmospheric Sciences*, *38*, 1179–1196.

Hurrell, J. W. (1996). Influence of variations in extratropical wintertime teleconnections on Northern Hemisphere temperature. *Geophysical Research Letters*, *23*, 665–668. https://doi.org/10.1029/96GL00459

Jiang, Z., Feldstein, S. B., & Lee, S. (2017). The relationship between the Madden-Julian Oscillation and the North Atlantic Oscillation. *Quarterly Journal of the Royal Meteorological Society*, *143*, 240–250. https://doi.org/10.1002/qj.2917

Karpechko, A. Y., Hitchcock, P., Peters, D. H. W., & Schneidereit, A. (2017). Predictability of downward propagation of major sudden stratospheric warmings. *Quarterly Journal of the Royal Meteorological Society*, *143*, 1459–1470. https://doi.org/10.1002/qj.3017

Kessler, W. S. (2001). EOF representations of the Madden-Julian Oscillation and its connection with ENSO. *Journal of Climate*, *14*, 3055–3061. https://doi.org/10.1175/1520-0442(2001)014<3055:EROTMJ>2.0.CO;2

Kidston, J., Scaife, A. A., Hardiman, S. C., Mitchell, D. M., Butchart, N., Baldwin, M. P., & Gray, L. J. (2015). Stratospheric influence on tropospheric jet streams, storm tracks and surface weather. *Nature Geoscience*, *8*, 433–440. https://doi.org/10.1038/NGEO2424

Kiladis, G. N., Dias, J., Straub, K. H., Wheeler, M. C., Tulich, S. N., Kikuchi, K., et al. (2014). A comparison of OLR and circulation-based indices for tracking the MJO. *Monthly Weather Review*, *142*, 1697–1715. https://doi.org/10.1175/MWR-D-13-00301.1

Kodera, K. (2006). Influence of stratospheric sudden warming on the equatorial troposphere. *Geophysical Research Letters*, *33*, L06804. https://doi.org/10.1029/2005GL024510

L'Heureux, M. L., & Higgins, R. W. (2008). Boreal winter links between the Madden–Julian oscillation and the Arctic oscillation. *Journal of Climate*, *21*, 3040–3050. https://doi.org/10.1175/2007JCLI1955.1

Lau, W. K.-M., & Waliser, D. E. (2012). *Intraseasonal variability in the atmosphere-ocean climate system*. Berlin Heidelberg: Springer-Verlag. https://doi.org/10.1007/978-3-642-13914-7

Lin, H., Brunet, G., & Derome, J. (2009). An observed connection between the North Atlantic Oscillation and the Madden–Julian oscillation. *Journal of Climate*, *22*, 364–380. https://doi.org/10.1175/2008JCLI2515.1

Madden, R. A., & Julian, P. R. (1971). Detection of a 40–50 day oscillation in the zonal wind in the tropical Pacific. *Journal of the Atmospheric Sciences*, *28*, 702–708.

Madden, R. A., & Julian, P. R. (1994). Oscillation of the 40–50-day tropical oscillation—A review. *Monthly Weather Review*, *122*, 814–837.

Matsuno, T. (1971). A dynamical model of the stratospheric sudden warming. *Journal of the Atmospheric Sciences*, *28*, 1479–1494. https://doi.org/10.1175/1520-0469(1971)028<1479:ADMOTS>2.0.CO;2

Matthews, A. J., Hoskins, B. J., & Masutani, M. (2004). The global response to tropical heating in the Madden–Julian Oscillation during the northern winter. *Quarterly Journal of the Royal Meteorological Society*, *130*, 1991–2011. https://doi.org/10.1256/qj.02.123

Moore, R. W., Martius, O., & Spengler, T. (2010). The modulation of the subtropical and extratropical atmosphere in the Pacific basin in response to the Madden–Julian oscillation. *Monthly Weather Review*, *138*, 2761–2779. https://doi.org/10.1175/2010MWR3194.1

Mori, M., & Watanabe, M. (2008). The growth and triggering mechanisms of the PNA: A MJO-PNA coherence. *Journal of the Meteorological Society of Japan*, *86*, 213–236.

Riddle, E. E., Butler, A. H., Furtado, J. C., Cohen, J. L., & Kumar, A. (2013). CFSv2 ensemble prediction of the wintertime Arctic Oscillation. *Climate Dynamics*, *41*, 1099–1116. https://doi.org/10.1007/s00382-013-1850-5

Roundy, P. E. (2012). Chapter 14: Tropical-extratropical interactions. *Intraseasonal Variability of the Atmosphere-Ocean Climate System*, *2*, 497–512.

Roundy, P. E., Schreck, C. J., & Janiga, M. A. (2009). Contributions of convectively coupled equatorial Rossby waves and Kelvin waves to the real-time multivariate MJO indices. *Monthly Weather Review*, *137*, 469–478. https://doi.org/10.1175/2008MWR2595.1

Rui, H., & Wang, B. (1990). Development characteristics and dynamic structure of tropical intraseasonal convective anomalies. *Journal of the Atmospheric Sciences*, *47*, 357–379.

Scaife, A. A., Arribas, A., Blockley, E., Brookshaw, A., Clark, R. T., Dunstone, N., et al. (2014). Skillful long-range prediction of European and North American winters. *Geophysical Research Letters*, *41*, 2514–2519. https://doi.org/10.1002/2014GL059637

Scaife, A. A., Yu Karpechko, A., Baldwin, M. P., Brookshaw, A., Butler, A. H., Eade, R., et al. (2016). Seasonal winter forecasts and the stratosphere. *Atmospheric Science Letters*, *17*, 51–56. https://doi.org/10.1002/asl.598

Schwartz, C., & Garfinkel, C. I. (2017). Relative roles of the MJO and the stratospheric variability in North Atlantic and European winter climate. *Journal of Geophysical Research: Atmospheres*, *122*, 4184–4201. https://doi.org/10.1002/2016JD025829

Seo, K.-H., & Lee, H.-J. (2017). Mechanisms for a PNA-like teleconnection pattern in response to the MJO. *Journal of the Atmospheric Sciences*, *74*, 1767–1781. https://doi.org/10.1175/JAS-D-16-0343.1

Seo, K.-H., Lee, H.-J., & Frierson, D. M. W. (2016). Unraveling the teleconnection mechanisms that induce wintertime temperature anomalies over the Northern Hemisphere continents in response to the MJO. *Journal of the Atmospheric Sciences*, *73*, 3557–3571. https://doi.org/10.1029/98GL00950

Thompson, D. W. J., Baldwin, M. P., & Wallace, J. M. (2002). Stratospheric connection to Northern Hemisphere wintertime weather: Implications for prediction. *Journal of Climate*, *15*, 1421–1428.

Thompson, D. W. J., Furtado, J. C., & Shepherd, T. G. (2006). On the tropospheric response to anomalous stratospheric wave drag and radiative heating. *Journal of the Atmospheric Sciences*, *63*, 2616–2629.

Thompson, D. W. J., & Wallace, J. M. (1998). The Arctic oscillation signature in the wintertime geopotential height and temperature fields. *Geophysical Research Letters*, *25*, 1297–1300. https://doi.org/10.1029/98GL00950

Thompson, D. W. J., & Wallace, J. M. (2000). Annular modes in the extratropical circulation. Part I: Month-to-month variability. *Journal of Climate*, *13*, 1000–1016.

Thompson, D. W. J., & Wallace, J. M. (2001). Regional climate impacts of the Northern Hemisphere annular mode. *Science*, *293*, 85–89.

Trenberth, K. E., Branstator, G. W., Karoly, D., Kumar, A., Lau, N.-C., & Ropelewski, C. (1998). Progress during TOGA in understanding and modeling global teleconnections associated with tropical sea surface temperatures. *Journal of Geophysical Research*, *103*, 14,291–14,324. https://doi.org/10.1029/97JC01444

Tseng, K.-C., Barnes, E. A., & Maloney, E. D. (2018). Prediction of the midlatitude response to strong Madden-Julian Oscillation events on S2S timescales. *Geophysical Research Letters*, *45*, 463–470. https://doi.org/10.1002/2017GL075734

Tseng, K.-C., Maloney, E., & Barnes, E. A. (2018). The consistency of MJO teleconnection patterns: An explanation using linear Rossby wave theory. *Journal of Climate*, *32*, 531–548. https://doi.org/10.1175/JCLI-D-18-0211.1

Vitart, F., Ardilouze, C., Bonet, A., Brookshaw, A., Chen, M., Codorean, C., et al. (2017). The Subseasonal to Seasona l (S2S) Prediction project database. *Bulletin of the American Meteorological Society*, *98*, 163–173. https://doi.org/10.1175/BAMS-D-16-0017.1

Vitart, F., Robertson, A. W., & Anderson, D. L. T. (2012). Subseasonal to seasonal prediction project: Bridging the gap between weather and climate. *World Meteorological Organization Bulletin*, *61*, 23–28.

Walker, G. T., & Bliss, E. W. (1932). Memoirs of the royal meteorological society. *World weather V*, *4*, 53–84.

Wang, L., Li, T., Chen, L., Behera, S. K., & Nasuno, T. (2018). Modulation of the MJO intensity over the equatorial western Pacific by two types of El Niño. *Climate Dynamics*, *51*, 687–700. https://doi.org/10.1007/s00382-017-3949-6

Waugh, D. W., Sobel, A. H., & Polvani, L. M. (2017). What is the polar vortex and how does it influence weather?*Bulletin of the American Meteorological Society*, *98*, 37–44. https://doi.org/10.1175/BAMS-D-15-00212.1

Weare, B. C. (2010). Extended Eliassen-Palm fluxes associated with the Madden-Julian oscillation in the stratosphere. *Journal of Geophysical Research*, *115*, D24103. https://doi.org/10.1029/2010JD014390

Wheeler, M. C., & Hendon, H. H. (2004). An all-season real-time multivariate MJO index: Development of an index for monitoring and prediction. *Monthly Weather Review*, *132*, 1917–1932.

Woollings, T., Hoskins, B., Blackburn, M., & Berrisford, P. (2008). A new Rossby wave–breaking interpretation of the North Atlantic Oscillation. *Journal of the Atmospheric Sciences*, *65*, 609–626. https://doi.org/10.1175/2007JAS2347.1

Zhang, C. (2005). Madden-Julian oscillation. *Reviews of Geophysics*, *43*, RG2003. https://doi.org/10.1029/2004RG000158

Zhou, S., L'Heureux, M., Weaver, S., & Kumar, A. (2012). A composite study of the MJO influence on the surface air temperature and precipitation over the Continental United States. *Climate Dynamics*, *38*, 1459–1471. https://doi.org/10.1007/s00382-011-1001-9

Zhou, S., & Miller, A. J. (2005). The interaction of the Madden-Julian oscillation and the Arctic oscillation. *Journal of Climate*, *18*, 143–159.